Research Article | Vol. 30, No. 19 / 12 Sep 2022 / Optics Express 34655

Optics EXPRESS

Planar Alvarez tunable lens based on polymetric liquid crystal Pancharatnam-Berry optical elements

SHUYI CHEN,[1] JUNHAO LIN,[1] ZIQIAN HE,[2] YAN LI,[1,*] YIKAI SU,[1] AND SHIN-TSON WU[2]

[1]Department of Electronic Engineering, Shanghai Jiao Tong University, Shanghai, China
[2]College of Optics and Photonics, University of Central Florida, Orlando, Florida 32816, USA
[*]yan.li@sjtu.edu.cn

Abstract: Virtual reality (VR) and augmented reality (AR) have widespread applications. The vergence-accommodation conflict (VAC), which causes 3D visual fatigue, has become an urgent challenge for VR and AR displays. Alvarez lenses, with precise and continuously tunable focal length based on the lateral shift of its two sub-elements, are a promising candidate as the key electro-optical component in vari-focal AR display systems to solve the VAC problem. In this paper, we propose and fabricate a compact Alvarez lens based on planar polymetric liquid crystal Pancharatnam-Berry optical elements. It can provide continuous diopter change from -1.4 D to 1.4 D at the wavelength of 532 nm with the lateral shift ranging from -5 mm to 5 mm. We also demonstrate an AR display system using this proposed Alvarez lens, where virtual images are augmented on the real world at different depths.

1. Introduction

Recently, the emergence of virtual reality (VR) and augmented reality (AR) technologies is revolutionizing the way we perceive and interact with the world [1,2]. VR and AR have been applied in areas including healthcare, education, entertainment, and military training. However, most of the commercial AR display products on the market suffer from the vergence-accommodation conflict (VAC) [3,4]. Each eye accommodates at a fixed distance, which is the image position of the micro display screen generated by the display optics, while the binocular visual axes of two eyes converge at the depth of virtual 3D objects. [5] This inconsistency inevitably induces 3D visual fatigue in these AR displays and leads to poor user experience [6]. Therefore, the exploration of new 3D display methods to effectively eliminate the VAC is crucial in the next generation of VR/AR display technologies.

There are several methods proposed to solve the VAC problem, including holographic display [7], light field display [8], and volumetric display [9]. Among them, vari-focal [10] and multi-focal display [11] technologies are two typical volumetric display technologies that have been applied in AR display systems. In a vari-focal display system, the depth of single-plane virtual objects could be dynamically adjusted, so that virtual objects appear to exist in different depths. In a multi-focal display system, multiple 2D cross sections of virtual objects can be rendered at multiple depths simultaneously to reconstruct a 3D volume. In both cases, the human eye can accommodate on the correct depths of the virtual objects. To realize a vari- or multi-focal display system, tunable lenses, such as deformable membrane devices [12], liquid crystal lenses [13], and electrowetting lenses [14], have been served as key components to alter image depth by varying their optical power. Dunn et al. [15] designed an optical see-through vari-focal AR display system using deformable beam splitter membranes. Liu et al. [16] realized an optical see-through head-mounted vari-focal 3D display device using a liquid lens. Kang et al. [14] presented a novel configuration of vari-focus liquid lens based on electrowetting-on-dielectric technique, and the

#468647 https://doi.org/10.1364/OE.468647
Journal © 2022 Received 23 Jun 2022; revised 1 Aug 2022; accepted 2 Aug 2022; published 8 Sep 2022

Optics EXPRESS

position and curvature of the liquid meniscus can be reversibly adjusted by varying the applied voltage. Wang et al. [17] demonstrated a novel design of a digitally switchable multi-focal lens composed of a freeform singlet and a customized programmable optical shutter array, showing the capability of rapidly switching the optical power of the system among multiple foci. Zhan et al. [18] and Li et al. [19] demonstrated compact vari-focal lenses for AR application, by stacking multiple fast-response liquid crystal lens elements; the optical power of such lenses can be conveniently tuned at high speed by electrically switching each element, with no mechanical moving component required; however, the focal length could only be switched among a few discrete values, but cannot be tuned continuously.

Alvarez lens [20–22], is a kind of tunable lens made of two sub-elements with complementary phase profiles. By laterally displacing the two sub-elements, its focal length can be continuously adjusted. Because of its large and continuously-tunable focal range, it is an attractive candidate as a key component for vari- and multi-focal display systems. Hua et al. [22] proposed and experimentally realized a novel design of an optical see-through vari-focal headed-mounted display system utilizing freeform Alvarez lenses, but such freeform Alvarez lenses requires highly precise manufacturing. Bawart et al. [23] demonstrated a modified configuration of an Alvarez lens using a $4f$-setup and a diffractive Alvarez element, and achieved focus tuning by rotating a galvo-mirror. However, the structure is still complicated and bulky for head-mounted display applications.

In this paper, we propose and demonstrate an ultrathin Alvarez tunable lens based on planar polymetric liquid crystal (PLC) Pancharatnam-Berry (PB) optical elements (PBOEs). The optical power of the proposed Alvarez lens can be continuously tuned from −1.4 diopters to 1.4 diopters when the lateral shift varies from −5 mm to 5 mm. Its focusing properties at different focal lengths are investigated, and imaging experiments are carried out to verify its vari-focal characteristic. With the planar Alvarez lens, we have also implemented a prototype of an AR display system, and experimentally demonstrated virtual images with good image quality augmented on the real world at different depths.

2. Working principle of the PLC Alvarez lens

The optical power of the Alvarez lens could be varied by laterally shifting its two identical planar PBOEs, as shown in Fig. 1(a)-(c). PBOEs [24,25] are a type of high-efficiency diffractive optical elements, that can be regarded as patterned half-wave plates. They are able to generate abrupt phase change based on their spatial variation of optical anisotropy. The structure of a PLC PBOE is shown in Fig. 1(d). A thin photoalignment layer [26] is sandwiched between the glass substrate and a PLC layer, and it reorientates the directors of the PLC to form a spatial variation in the x-y plane. When the thickness of the PLC layer satisfies half wave condition: $\Delta nd = m\lambda$, where Δn denotes the birefringence of the PLC material, d is the thickness of the PLC layer, m denotes an integer and λ is the wavelength of the incident light, circularly polarized light would be modulated by a PBOE as : [27]

$$\begin{aligned} J'_{out_\pm} &= R(-\theta)W(\pi)R(\theta)J_{in_\pm} \\ &= \begin{bmatrix} \cos\theta & -\sin\theta \\ \sin\theta & \cos\theta \end{bmatrix} \begin{bmatrix} e^{-i\frac{\pi}{2}} & 0 \\ 0 & e^{i\frac{\pi}{2}} \end{bmatrix} \begin{bmatrix} \cos\theta & \sin\theta \\ -\sin\theta & \cos\theta \end{bmatrix} \frac{1}{\sqrt{2}} \begin{bmatrix} 1 \\ \pm i \end{bmatrix} = -i\frac{1}{\sqrt{2}} \begin{bmatrix} 1 \\ \mp i \end{bmatrix} e^{\pm 2i\theta}, \end{aligned} \tag{1}$$

where J_{in+} and J_{in-} denote the Jones vectors of left-handed circularly polarized (LCP) and right-handed circularly polarized (RCP) incident light, respectively, $R(\cdot)$ denotes the rotation matrix, θ and $W(\cdot)$ are the orientation angle and retardation Jones matrix of the local PLC half-wave plate, respectively. One can see that LCP and RCP incident light experiences the same amount of phase shift 2θ but with opposite signs. Moreover, the circularly polarized light gets its handedness inversed after being modulated by the PBOE.

Optics EXPRESS

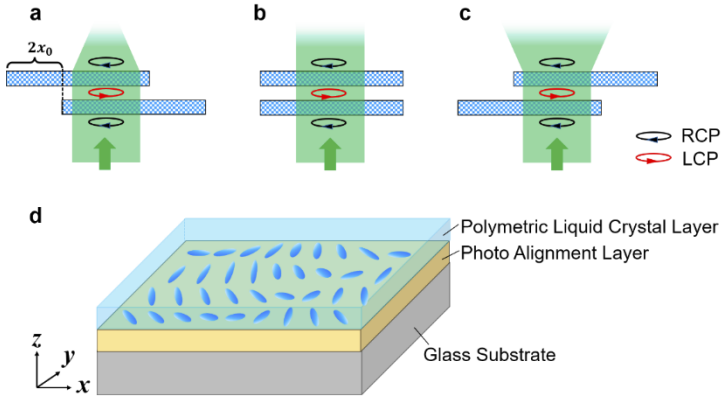

Fig. 1. Schematic illustration of the proposed Alvarez lens with a (a) positive, (b) zero or (c) negative optical power as the lateral shift varies. (d) Structure of a PLC PBOE.

Here, the LC orientation of the two identical PBOEs of the Alvarez lens is so designed that their corresponding phase shifts for RCP and LCP light are:

$$\varphi_{RCP}(x,y) = -\varphi_{LCP}(x,y) = 2\theta(x,y) = A(\frac{x^3}{3} + xy^2), \tag{2}$$

where x and y are the coordinates. Here A is a design parameter, which determines the focal length of the Alvarez lens. Assuming the incident light is RCP, then it would be converted to LCP light while gaining a phase modulation φ_{RCP}, after passing through the first sub-element. As for the second sub-element, since now the incident light is LCP, it provides a phase shift φ_{LCP} that is opposite the first sub-element, even though it has the identical LC orientation. If each sub-element is laterally shifted by a distance x_0 in the opposite direction, the overall phase modulation after passing through the two sub-elements of the Alvarez lens is:

$$\begin{aligned} \varphi_{Alvarez} &= \varphi_{RCP}(x - x_0, y) + \varphi_{LCP}(x + x_0, y) \\ &= A(\tfrac{(x-x_0)^3}{3} + (x - x_0)y^2) - A(\tfrac{(x+x_0)^3}{3} + (x + x_0)y^2) \\ &= -2Ax_0(x^2 + y^2) - \tfrac{2}{3}Ax_0^3 \\ &= -2Ax_0(x^2 + y^2) - \varphi_0 \end{aligned} \tag{3}$$

Here φ_0 is a constant global phase shift. According to the phase profile of a parabolic lens

$$\varphi_{Parabolic}(x,y) = -\frac{\pi}{\lambda f}(x^2 + y^2) + \varphi_C, \tag{4}$$

where λ denotes the wavelength, f denotes the focal length of the lens and φ_C is also a constant global phase shift, the focal length of the Alvarez lens can be expressed as:

$$f_{Alvarez} = \frac{\pi}{2\lambda A x_0} \tag{5}$$

It is clear that the focal length of the Alvarez tunable lens is inversely proportional to the lateral shift distance x_0. In other words, we can achieve the desired focal length range of the Alvarez lens by elaborately designing the parameter A. Figure 1(a)-(c) demonstrates that it can achieve a positive, zero or negative optical power with different lateral shift x_0.

Optics EXPRESS

3. Pancharatnam-Berry optical elements of the Alvarez lens

To validate our design, we fabricated two Alvarez PLC PB samples with the design wavelength of λ = 532 nm and $A = 0.84361$ mm^{-3}. First, a glass substrate was cleaned and then treated by UV-Ozone for 20 minutes. Next a photo-alignment layer was formed on the substrate by spin-coating a 0.2% solution of Brilliant Yellow (BY) in dimethylformamide (DMF) solvent at the speed of 500 rpm for 5s and then 3000 rpm for 30s. After being dried in a vacuum oven at 80 °C for 5 minutes, the sample was directly exposed using a single-exposure method [28], whose exposure setup is illustrated in Fig. 2. A 457 nm blue laser (Changchun New Industries, MSL-FN-457-300mW) is employed as the light source, and the SLM (HoloEye PLUTO-2.1) used here has a resolution of 1920 × 1080 and pixel size of 8 μm. The curve of PB phase versus grey levels is plotted in Fig. 3(a). Here, during the exposure process, we only chose 12 discrete phase values with an interval of π/6 to approximately represent the continuous phase distribution calculated by Eq. (2), and the quantized phase distribution is depicted in Fig. 3(b). After exposure, the sample was spin-coated with a diluted liquid crystal reactive mesogen mixture (RMM) solution in toluene solvent at 500 rpm for 5 s and then 2350 rpm for 30 s. The solution of RMM was mixed by 96% of the reactive mesogen RM257 and 4% of the photoinitiator Irgacure 651. After being spin-coated, the sample was cured by 365 nm UV light to form a thin cross-linked PLC film on the glass substrate [29].

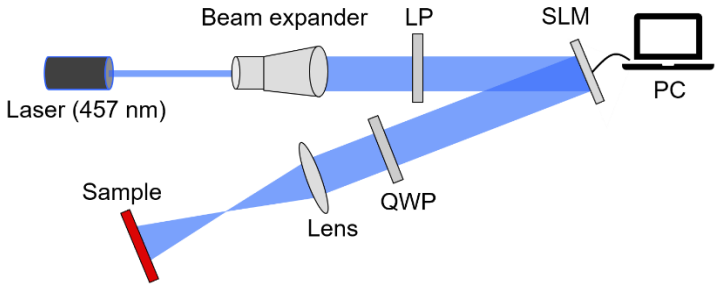

Fig. 2. Optical setup for the single-exposure method. LP denotes a linear polarizer and QWP denotes a quarter wave plate, SLM is the spatial light modulator and PC is a personal computer.

Figure 3(c) and (d) shows the polarization microscopic images of a fabricated sample. Both the peripheral part (Fig. 3(c)) and the central part (Fig. 3(d)) are consistent with the phase distribution depicted in Fig. 3(b). From the figures, we can find that the phase profile of each sub-element of the Alvarez lens is anti-symmetric in the x direction and symmetric in the y direction, which can also be deduced from Eq. (2). The size of our sample is about 1.65 cm x 1.05 cm. Larger-size samples could be achieved by employing tiling technique based on multiple exposures [30], or optimizing the exposure optical system and employing a SLM with higher resolution.

Since we set the parameter $A = 0.84361$ mm^{-3} and λ = 532 nm, the optical power of the proposed Alvarez lens should be tuned from −1.4 diopters to 1.4 diopters when the lateral shift ranges from −5 mm to 5 mm, which can be derived from Eq. (5). Figure 4(a) depicts the focal length of the proposed Alvarez lens as a function of the lateral shift of the two sub-elements. We performed the focusing experiment of this Alvarez lens using a collimated RCP HeNe laser beam (532 nm) with a diameter of 5 mm. As we gradually increased the lateral shift x_0 in one direction (x_0>0), the output beam became more and more convergent, indicating an increased positive optical power. And when we gradually shifted in the other direction (x_0<0), the beam got more and more divergent, as a stronger negative optical power was achieved. We captured pictures of the focal spots using a charge-coupled device (CCD) camera when the Alvarez lens had a positive power, so as to evaluate its focusing property. Figure 4(b)-(e) shows the CCD pictures taken at

Optics EXPRESS

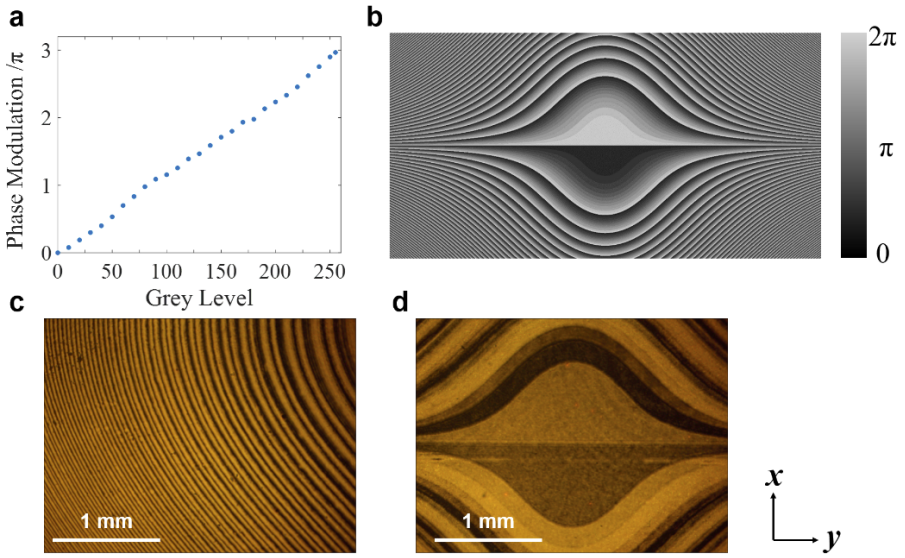

Fig. 3. (a) PB phase modulation versus grey levels. (b) Phase distribution of a sub-element. Microscopic images of the sample: (c) the peripheral section and (d) the central section of the sample.

the focal plane of the lens, when x_0 is 3 mm, 3.5 mm, 4.5 mm and 5 mm, respectively. One could tell from Fig. 4 that light could be focused at different distance, indicating different focal length as x_0 changes. The spot sizes are a bit larger than the diffraction-limited values because of measurement error or fabrication imperfection.

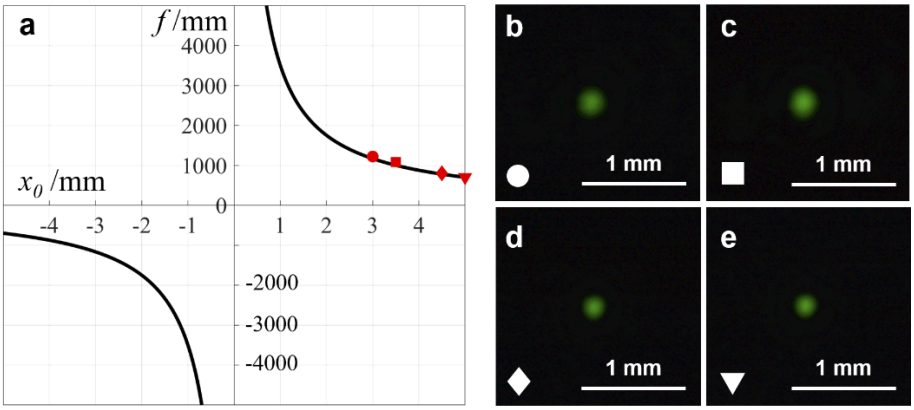

Fig. 4. (a) Focal length f as a function of the lateral shift x_0. Black curve–theoretical curve. Red symbols-experimental data. Corresponding focal spots when (b) $x_0 = 3$ mm, (c) $x_0 = 3.5$ mm, (d) $x_0 = 4.5$ mm and (e) $x_0 = 5$ mm.

To further verify the vari-focal characteristic of the Alvarez lens, we employed the sample in a simple imaging system. The optical setup is shown in Fig. 5. Illuminated by a green LED light source, a patterned mask with a letter "G" is placed at a proper position as the image source. After passing through a circular polarizer, the image light is converted to RCP light. Then a refractive lens (Lens1: $f = 25$ cm) is used to adjust the object distance of the Alvarez lens. By laterally shifting the sub-elements of the Alvarez lens, image is generated at different distances.

Optics EXPRESS

So clear or blurry imaging results can be observed when placing the receiving screen at different distances.

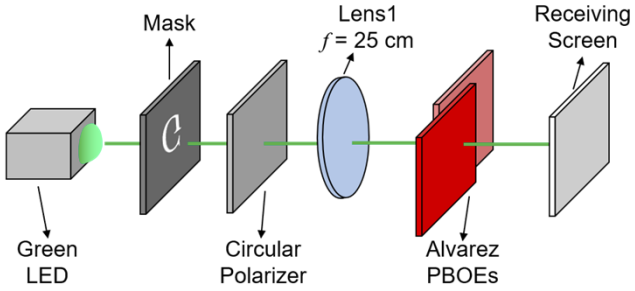

Fig. 5. Optical setup for the imaging system with the Alvarez PBOEs.

Here, the mask is placed 50 cm in front of the Lens1, which is twice the focal length of the refractive lens. The distance between the Alvarez lens and Lens1 is 20 cm, and we assume that the position of the Alvarez tunable lens is $z = 0$. When the lateral shift of the two sub-elements $x_0 = 0$, the diopter of the Alvarez lens is 0. At this time, the image of the mask is simply generated at a distance of 30 cm after the Alvarez lens. A clear real image of the letter "G" can be observed when the receiving screen is placed at $z = 30$ cm, as shown in Fig. 6(e). But when the screen is placed at other distances (Fig. 6(d) and (f)), the images get blurry. When the lateral shift $x_0 = -5$ mm, the diopter of the Alvarez lens is changed to -1.4 D. As shown in Fig. 6(a)-(c), the letter "G" is clear at $z = 21$ cm and blurry at other distances. When $x_0 = 5$ mm, the diopter of the Alvarez

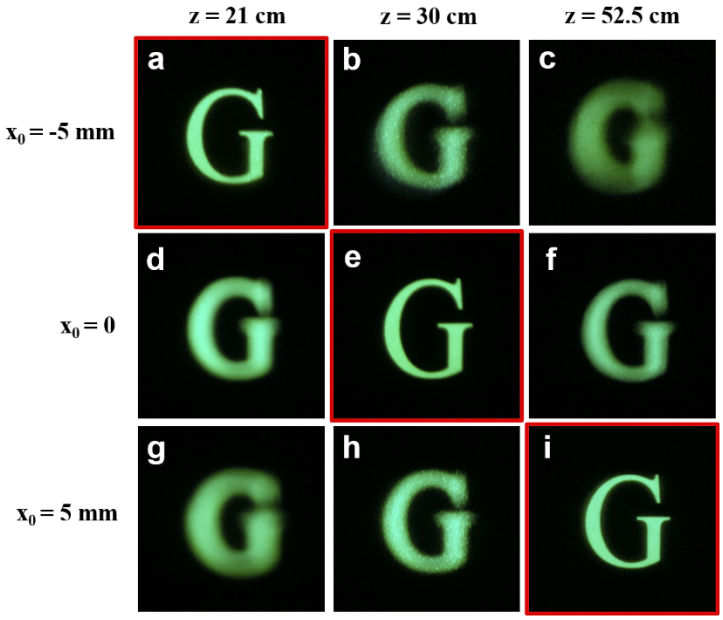

Fig. 6. Imaging results with different lateral shifts. (a-c) Images captured at (a) $z = 21$ cm, (b) $z = 30$ cm and (c) $z = 52.5$ cm, respectively, when the lateral shift $x_0 = -5$ mm. (d-f) Images captured at (d) $z = 21$ cm, (e) $z = 30$ cm and (f) $z = 52.5$ cm, respectively, when the lateral shift $x_0 = 0$. (g-i) Images captured at (g) $z = 21$ cm, (h) $z = 30$ cm and (i) $z = 52.5$ cm, respectively, when the lateral shift $x_0 = 5$ mm.

Optics EXPRESS

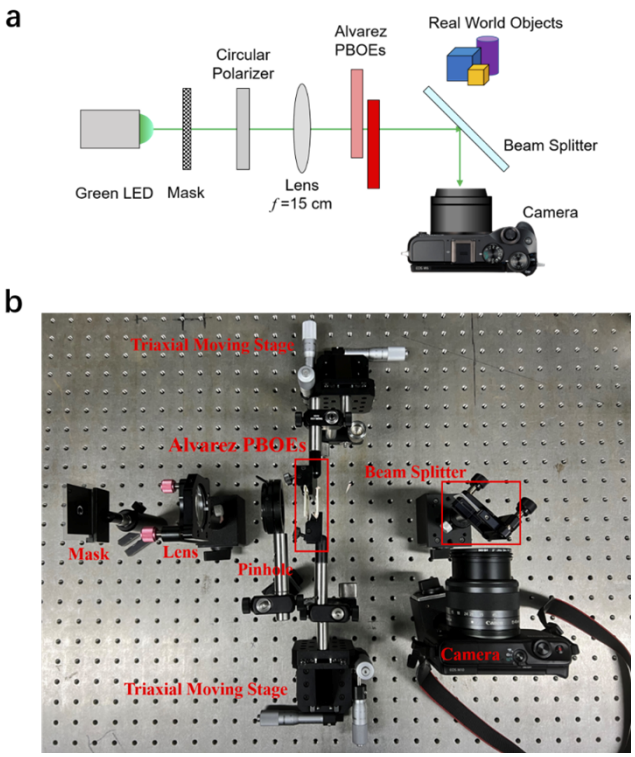

Fig. 7. (a) Diagram of the experimental setup for the prototype of an AR display system using the proposed Alvarez lens. (b) Photo of the optical components of the AR display prototype on an optical table.

lens is changed to 1.4 D, and the image is quite clear at $z = 52.5$ cm (Fig. 6(i)) but blurry at both $z = 21$ cm (Fig. 6(g)) and $z = 30$ cm (Fig. 6(h)). In summary, our Alvarez lens demonstrates vari-focal capability and can adjust the depth of images in the imaging system.

Vari-focal display technology can adjust the depth of the image plane, so that virtual objects can be displayed at proper depths, which is one of the effective solutions to solve the VAC problem. The Alvarez tunable lens possesses precise and continuous focusing characteristics and can be applied in vari-focal AR display system. So we employed the fabricated Alvarez lens in a proof-of-concept prototype of an AR display system. The optical setup is shown in Fig. 7. A patterned mask with a letter "G" illuminated by a green LED is also set as the image source. Here, the focal length of the refractive lens is 15 cm, and the mask is placed 10 cm in front of it. The distances between the refractive lens and the Alvarez lens, the Alvarez lens and the beam splitter, the beam splitter and the camera are 10 cm, 12 cm and 3 cm, respectively. Similarly, we changed the lateral shift of the two sub-elements to tune the focal length of the Alvarez lens and the image distance. Figure 8 shows the pictures taken by the camera in three exemplary cases when the virtual image was rendered at 40 cm, 55 cm and 70 cm, respectively. Due to the use of the beam splitter, one can observe the augmentation of a virtual image "G" on the real-world scene that has three brackets with notes tagged on them. The notes indicate that the brackets are placed at 40 cm, 55 cm and 70 cm away from the camera, respectively. In Fig. 8(a)-(c), when the lateral shift x_0 is -5 mm, the focal length of the Alvarez lens is -70 cm for RCP incidence. According to the lens equation, the virtual image should be generated at a distance of 40 cm away from the camera theoretically. From the enlarged images, one can see that the image is quite clear

Optics EXPRESS

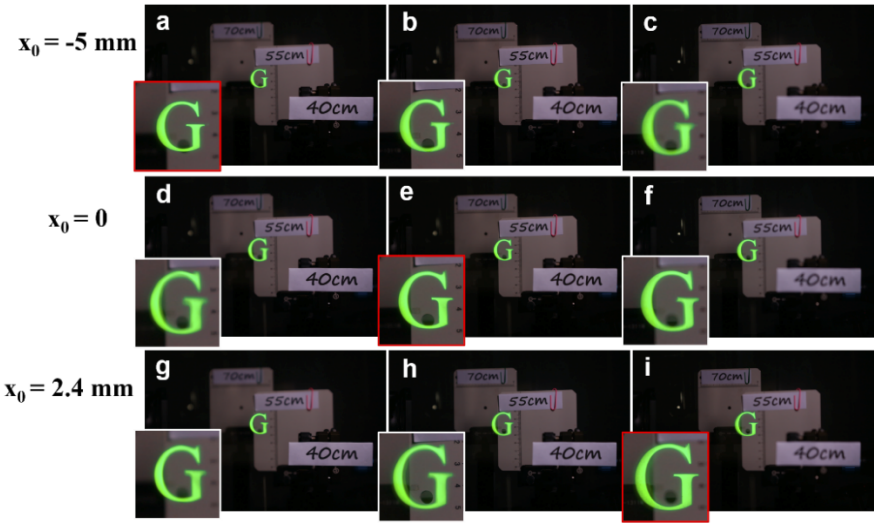

Fig. 8. Augmented reality imaging results with different lateral shifts. (a-c) Images captured when the lateral shift $x_0 = -5$ mm, and the camera is focused at (a) 40 cm, (b) 55 cm and (c) 70 cm, respectively. (d-f) Images captured when the lateral shift $x_0 = 0$, and the camera is focused at (d) 40 cm, (e) 55 cm and (f) 70 cm, respectively. (g-i) Images captured when the lateral shift $x_0 = 2.4$ mm, and the camera is focused at (g) 40 cm, (h) 55 cm and (i) 70 cm, respectively.

at the depth of 40 cm but relatively blurry at the depths of 55 cm and 70 cm. In Fig. 8(d)-(f), x_0 is set to be 0, and the virtual image should appear at 55 cm away from the camera. Indeed when the camera is focused at the depth of 55 cm, the virtual "G" is rather clear, but when the camera is focused at other distances, it is blurry. And in Fig. 8(g)-(i), when the lateral shift is changed to 2.4 mm, the focal length of the Alvarez lens becomes 145.8 cm. The virtual image does not become clear until the focusing depth achieves 70 cm. The above experimental results verify that the Alvarez tunable lens based on PBOEs can adjust the focal length by the lateral shift of the sub-elements. This vari-focal device enables virtual objects to be displayed at proper depths so that the human eye does not need to focus on a fixed display screen, which is of great benefit to solve the VAC problem and reduce visual fatigue.

In the proof-of-concept AR display system, which is mostly based on off-the-shelf optical elements, the depth range is not optimized yet. It could be further extended by optimizing the optical system configuration as well as the Alvarez lens parameters. The current Alvarez PB lens design is optimized for 532 nm wavelength and its focal length would vary as wavelength changes. To be used for color AR display systems, achromatic PB lens design [31] or additional compensation methods [32,33] would be required to suppress chromatic dispersion. Although in our experiment the lateral displacement control is done manually, it could be realized by electric motion control devices [22], to achieve more accurate, convenient and faster vari-focal characteristics, providing more realistic and dynamic 3D AR experience.

4. Conclusion

In this work, we have proposed and experimentally demonstrated an ultrathin Alvarez tunable lens based on PLC PBOEs. The planar Alvarez lens is capable of adjusting its optical power continuously from −1.4 diopters to 1.4 diopters as the lateral shift of the two sub-elements varies from −5 mm to 5 mm. Imaging experiments were conducted to verify the vari-focal characteristic

Optics EXPRESS

of the Alvarez lens. We further employed the Alvarez lens in an AR display system to carry out the imaging experiments of virtual images augmented on the real world at different depths. Such a device provides continuous and accurate focus adjustment within a large focal range, while maintaining an ultra-thin form factor. Thus, it is attractive for vari- or multi-focal AR display systems to address the VAC problem, and is of great significance in the application of head-mounted AR display systems.

Funding. National Key Research and Development Program of China (2021YFB2802100); National Natural Science Foundation of China (61727808, 62075127).

Disclosures. The authors declare no conflicts of interest.

Data availability. Data underlying the results presented in this paper are not publicly available at this time but may be obtained from the authors upon reasonable request.

References

1. J. Xiong, E. L. Hsiang, Z. He, T. Zhan, and S.-T. Wu, "Augmented reality and virtual reality displays: emerging technologies and future perspectives," Light: Sci. Appl. **10**(1), 216 (2021).
2. J. Xiong and S.-T. Wu, "Planar liquid crystal polarization optics for augmented reality and virtual reality: from fundamentals to applications," eLight **1**(1), 3 (2021).
3. J. Geng, "Three-dimensional display technologies," Adv. Opt. Photonics **5**(4), 456–535 (2013).
4. H. Hua and B. Javidi, "A 3D integral imaging optical see-through head-mounted display," Opt. Express **22**(11), 13484–13491 (2014).
5. S. Chen, Y. Li, S. Liu, and Y. Su, "3D-visual fatigue-free AR displays," Proc. SPIE **12024**, 66–74 (2022).
6. D. M. Hoffman, A. R. Girshick, K. Akeley, and M. S. Banks, "Vergence-accommodation conflicts hinder visual performance and cause visual fatigue," J. Vis. **8**(3), 33 (2008).
7. P. Zhou, Y. Bi, M. Sun, H. Wang, F. Li, and Y. Qi, "Image quality enhancement and computation acceleration of 3D holographic display using a symmetrical 3D GS algorithm," Appl. Opt. **53**(27), G209–G213 (2014).
8. H. Huang and H. Hua, "Systematic characterization and optimization of 3D light field displays," Opt. Express **25**(16), 18508–18525 (2017).
9. S. Liu, Y. Li, P. Zhou, X. Li, N. Rong, S. Huang, W. Lu, and Y. Su, "A multi-plane optical see-through head mounted display design for augmented reality applications," J. Soc. Inf. Disp. **24**(4), 246–251 (2016).
10. H. Hua, "Enabling focus cues in head-mounted displays," Proc. IEEE **105**(5), 805–824 (2017).
11. X. Hu and H. Hua, "Design and assessment of a depth-fused multi-focal-plane display prototype," J. Disp. Technol. **10**(4), 308–316 (2014).
12. M. J. Moghimi, B. J. Lutzenberger, B. M. Kaylor, and D. L. Dickensheets, "MOEMS deformable mirrors for focus control in vital microscopy," J. Micro. Nanolithogr. MEMS. MOEMS. **10**(2), 023005 (2011).
13. S. Suyama, M. Date, and H. Takada, "Three-dimensional display system with dual-frequency liquid-crystal varifocal lens," Jpn. J. Appl. Phys. **39**(Part 1, No. 2A), 480–484 (2000).
14. M. Kang and R. Yue, "Variable-focus liquid lens based on EWOD," J. Adhes. Sci. Technol. **26**(12-17), 1941–1946 (2012).
15. D. Dunn, P. Chakravarthula, Q. Dong, and H. Fuchs, "Mitigating vergence-accommodation conflict for near-eye displays via deformable beamsplitters," Proc. SPIE **10676**, 196–208 (2018).
16. S. Liu, H. Hua, and D. Cheng, "A novel prototype for an optical see-through head-mounted display with addressable focus cues," IEEE Trans. Vis. Comput. Graph. **16**(3), 381–393 (2009).
17. X. Wang, Y. Qin, H. Hua, Y. H. Lee, and S.-T. Wu, "Digitally switchable multi-focal lens using freeform optics," Opt. Express **26**(8), 11007–11017 (2018).
18. T. Zhan, Y. H. Lee, and S.-T. Wu, "High-resolution additive light field near-eye display by switchable Pancharatnam-Berry phase lenses," Opt. Express **26**(4), 4863–4872 (2018).
19. S. Li, Y. Liu, Y. Li, S. Liu, S. Chen, and Y. Su, "Fast-response Pancharatnam-Berry phase optical elements based on polymer-stabilized liquid crystal," Opt. Express **27**(16), 22522–22531 (2019).
20. A. W. Lohmann, "A new class of varifocal lenses," Appl. Opt. **9**(7), 1669–1671 (1970).
21. L. Lu, F. Peng, W. S. T. Lam, and S. C. McEldowney, "Liquid crystal Alvarez lens," U.S. Patent 10,877,277 (29 December 2020).
22. A. Wilson and H. Hua, "Design and demonstration of a vari-focal optical see-through head-mounted display using freeform Alvarez lenses," Opt. Express **27**(11), 15627–15637 (2019).
23. M. Bawart, A. Jesacher, P. Zelger, S. Bernet, and M. Ritsch-Marte, "Modified Alvarez lens for high-speed focusing," Opt. Express **25**(24), 29847–29855 (2017).
24. S. Pancharatnam, "Generalized theory of interference and its applications," Proc. - Indian Acad. Sci., Sect. A **44**(6), 398–417 (1956).
25. M. V. Berry, "Quantal phase factors accompanying adiabatic changes," Proc. R. Soc. Lond. A **392**(1802), 45–57 (1984).

Optics EXPRESS

26. V. Presnyakov, K. Asatryan, T. Galstian, and V. Chigrinov, "Optical polarization grating induced liquid crystal micro-structure using azo-dye command layer," Opt. Express **14**(22), 10558–10564 (2006).
27. Y.-H. Lee, G. Tan, T. Zhan, Y. Weng, G. Liu, F. Gou, F. Peng, N. V. Tabiryan, S. Gauza, and S.-T. Wu, "Recent progress in Pancharatnam-Berry phase optical elements and the applications for virtual/augmented realities," Opt. Data Process. Stor. **3**(1), 79–88 (2017).
28. Y. Li, Y. Liu, S. Li, P. Zhou, T. Zhan, Q. Chen, Y. Su, and S.-T. Wu, "Single-exposure fabrication of tunable Pancharatnam-Berry devices using a dye-doped liquid crystal," Opt. Express **27**(6), 9054–9060 (2019).
29. T. Zhan, J. Xiong, Y. H. Lee, R. Chen, and S.-T. Wu, "Fabrication of Pancharatnam-Berry phase optical elements with highly stable polarization holography," Opt. Express **27**(3), 2632–2642 (2019).
30. X. J. Zhang, X. Zhou, Z. X. Yang, L. X. Zhang, W. Huang, and L. Chen, "High-throughput and controllable manufacturing of liquid crystal polymer planar microlens array for compact fingerprint imaging," Opt. Express **30**(2), 3101–3112 (2022).
31. Z. Zhao, M. Pu, H. Gao, J. Jin, X. Li, X. Ma, Y. Wang, P. Gao, and X. Luo, "Multispectral optical metasurfaces enabled by achromatic phase transition," Sci. Rep. **5**(1), 15781 (2015).
32. T. Zhan, J. Zou, J. Xiong, X. Liu, H. Chen, J. Yang, S. Liu, Y. Dong, and S.-T. Wu, "Practical chromatic aberration correction in virtual reality displays enabled by cost-effective ultra-broadband liquid crystal polymer lenses," Adv. Opt. Mater. **8**(2), 1901360 (2020).
33. G. Y. Lee, J. Y. Hong, S. Hwang, S. Moon, H. Kang, S. Jeon, H. Kim, J. H. Jeong, and B. Lee, "Metasurface eyepiece for augmented reality," Nat. Commun. **9**(1), 4562 (2018).